Molecular Dynamics Simulation of Desulfurization by Ionic Liquids

Xiaomin Liu
State Key Laboratory of Multiphase Complex Systems, Institute of Process Engineering, Chinese Academy of Sciences, Beijing 100080, China

Guohui Zhou
Beijing Shengjinqiao Information Technology Co., Ltd., Beijing 100083, China

Xiangping Zhang, and Suojiang Zhang
State Key Laboratory of Multiphase Complex Systems, Institute of Process Engineering, Chinese Academy of Sciences, Beijing 100080, China

DOI 10.1002/aic.12185
Published online April 20, 2010 in Wiley Online Library (wileyonlinelibrary.com).

Ionic liquids (ILs) have shown an excellent performance for removing the sulfur compounds of fuel. In this work, molecular dynamic simulations were performed to screen suitable IL instead of the traditional method which is inefficient. DBT and $DBTO_2$ were used as model compounds to study the mechanism of desulphurization. An all-atom force field was proposed for dibenzothiophene (DBT) and dibenzothiophene 5,5-dioxide ($DBTO_2$). The calculated results are in good agreement with the experimental value. We investigated the interaction between the model compounds and a series of ILs composed of 1-alkyl-3-methylimidazolium cations ($[C_{nmim}]^+$, n = 4, 6, 8, 10) and BF_4^-, PF_6^- anions. We found that the interaction between hydrogen atoms in imidazolium ring and oxygen atoms in $DBTO_2$ is stronger than that of sulfur atoms in DBT, and it means that $DBTO_2$ is extracted by ILs more easily than DBT. In this work, we also compared and discussed the desulphurization mechanism as a function of different ILs, sulfur contents, temperatures, and inclusion of water or not. The above results may help us design extractant and improve the operating conditions. © 2010 American Institute of Chemical Engineers *AIChE J,* 56: 2983–2996, 2010
Keywords: ionic liquids, molecular dynamics, desulphurization, extractant

Introduction

Deep desulphurization is of becoming more and more important, and new clean technologies with lower energy consumption are urgently needed, as lower sulfur-contained transportation fuel could greatly reduce the serious environmental pollutions, such as acid rain. However, traditional hydrodesulfurization has some drawbacks, such as high temperature and high pressure, high energy consumption, and difficulty in removing thiophenic compounds. In recent years, ionic liquids (ILs) have shown excellent performance for removing sulfur compounds from transportation fuels with the evident advantages such as mild operation conditions, no hydrogen needed, environmentally friendly, and deep desulfurization capacities.[1–9] Nie et al.[6] carried out systemic experiments and showed the desulfurization ability of three ILs and the selectivity with S-compounds. Zhang et al.[4] also performed serious experiments and they found $AlCl_3$-TMAC ILs has remarkably high-absorption capacities for aromatics. However, screening and designing suitable

Correspondence concerning this article should be addressed to S. Zhang at sjzhang@home.ipe.ac.cn.

Table 1. Force Field Parameters for DBT and $DBTO_2$

van der Waals parameters

Atoms	σ_i (Å)	ε_i (kJ mol^{-1})	Source	Description
CA	3.3997	0.3598	AMBER	Aromatic sp^2 carbon
CA^S	3.3997	0.3598	AMBER	Aromatic sp^2 carbon
CA^T	3.3997	0.3598	AMBER	Aromatic sp^2 carbon
HA	2.5996	0.0628	AMBER	H attached to aromatic carbon
S	3.5636	1.0460	AMBER	Sulfur in DBT or $DBTO_2$
O2	2.9599	0.8786	AMBER	sp^2 oxygen in anionic acids

Charges*

	$q(e)$			$q(e)$	
Atoms	DBT	$DBTO_2$	Atoms	DBT	$DBTO_2$
CA^S	0.0407	−0.0036	CA^T	0.0424	0.0144
CA^1	−0.1593	−0.1108	HA^1	0.1351	0.1200
CA^2	−0.1399	−0.1043	HA^2	0.1361	0.1253
CA^3	−0.1589	−0.1222	HA^3	0.1399	0.1267
CA^4	−0.1657	−0.1168	HA^4	0.1703	0.1664
S	−0.0814	0.7994	O2		−0.4948

Bond parameters

		r_0 (Å)		
Bonds	K_r (kJ mol^{-1} Å^{-2})	DBT	$DBTO_2$	Source
CA-CA	1589.92	1.397/1.385[†,‡]	1.400	This work
CA-CA^S	1589.92	1.398/1.386[†]	1.387	This work
CA-CA^T	1589.92	1.405/1.392[†]	1.398	This work
CA^S-CA^T	1589.92	1.414/1.409[†]	1.402	This work
CA^T-CA^T	1380.72	1.456/1.441[†]	1.480	This work
CA^S-S	1192.44	1.767/1.740[†]	1.803	This work
CA-HA	1569.00	1.087	1.086	This work
O2-S	2301.20		1.473	This work

Angle parameters

		θ_0 (deg.)		
Angles	K_0 (kJ mol^{-1} rad^{-2})	DBT	$DBTO_2$	Source
CA-CA-CA	259.408	120.6/120.5[†,§]	120.6	This work
CA-CA-CA^S	259.408	118.6/117.8[†]	117.8	This work
CA-CA-CA^T	259.408	119.8/120.0[†]	119.4	This work
CA-CA^S-CA^T	259.408	121.6/121.6[†]	123.1	This work
CA-CA^T-CA^S	259.408	118.8/118.7[†]	118.4	This work
CA-CA^T-CA^T	259.408	129.1/129.4[†]	128.3	This work
CA^S-CA^T−CA^T	259.408	112.1/111.9[†]	113.3	This work
CA^T-CA^S-S	259.408	112.4/112.3[†]	110.9	This work
CA-CA^S-S	259.408	126.0/126.1[†]	126.0	This work
CA^S-S-CA^S	271.960	91.0/91.5[†]	96.7	This work
CA-CA-HA	158.992	119.9	120.0	This work
CA^S-CA-HA	158.992	120.8	121.0	This work
CA^T-CA-HA	158.992	120.1	120.6	This work
CAS-S-O2	271.960		110.7	This work
O2-S-O2	271.960		119.0	This work

Dihedral parameters

Torsions	γ (deg)	K_ϕ (kJ mol^{-1})	n	Source
X-CA-CA-X	180	11.025	2	This work
X-CA-CA^S-X	180	11.025	2	This work
X-CA-CA^T-X	180	11.025	2	This work
X-CA^S-CA^T-X	180	11.025	2	This work
X-CA^T-CA^T-X	180	11.025	2	This work
X-CA^S-S-X	180	2.364	2	This work

Improper torsions

Torsions	γ (deg)	K_ϕ (kJ mol^{-1})	n	Source
CA-CA-CA-HA	180	4.602	2	This work

*The superscript of CA^1, CA^2, CA^3, and CA^4 is for marking the different charge, their atom type is CA. It is same for HA^1, HA^2, HA^3, and HA^4.
[†]Experimental data come from Ref. 25.
[‡]Experimental values for CA-CA are 1.385, 1.384, and 1.370, respectively.
[§]Experimental values for CA-CA-CA are 120.5 and121.6, respectively.

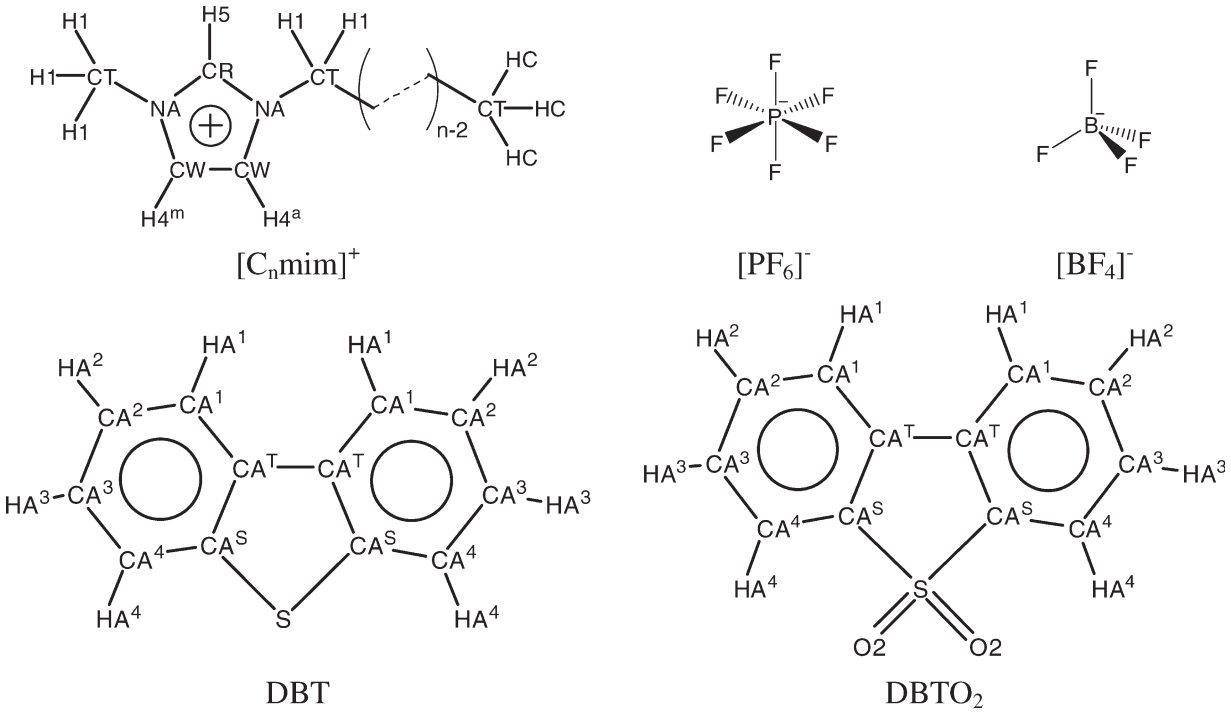

Figure 1. The structure of ILs and sulfur model compounds.

ILs for desulphurization from numerous ILs is still a great challenge, and the traditional method needs a large number of experiments. Fortunately, it has been shown that molecular simulation is one of the effective ways to analyze the intermolecular interactions in ILs.[10–18] However, no research on desulfurization using ILs using molecular dynamics (MD) simulations has been reported yet, and the desulfurization mechanism researches based on molecular scale will help to screen and design new and high-efficiency ILs extractants.

Dibenzothiophene (DBT) is one of the most common sulfur compounds in fuels, and it is hard to remove from fuel oil.[8] In this work, DBT and its corresponding oxide sulfone dibenzothiophene 5,5-dioxide ($DBTO_2$) are used as model compounds to study the mechanism of desulphurization using MD simulations. First, we set up all-atom force fields for DBT and $DBTO_2$ based on AMBER.[19] The calculated densities of DBT and $DBTO_2$ were used to validate the force field, and a good agreement with experimental densities was obtained. It is found that the interaction between hydrogen atoms in the imidazolium ring and oxygen atoms in $DBTO_2$ is stronger than that of the sulfur atoms in DBT. This is why $DBTO_2$ is extracted more easily than DBT by these ILs. Second, we analyzed several factors, including structures of ILs (side chain length and anion types), properties of fuel oil (sulfur and water content), and operating temperature. The conclusions may have some effects on selection of extractant and improving the operating conditions.

Force Field Development

The AMBER force field[19] was used with the following functional form for the potential energy E:

$$E = \sum_{\text{bonds}} K_r(r - r_0)^2 + \sum_{\text{angles}} K_\theta(\theta - \theta_0)^2 + \sum_{\text{torsions}} \frac{K_\phi}{2}(1 + \cos(n\phi - \gamma)) + \sum_{i=1}^{N}\sum_{j=i+1}^{N}\left\{4\varepsilon_{ij}\left[\left(\frac{\sigma_{ij}}{R_{ij}}\right)^{12} - \left(\frac{\sigma_{ij}}{R_{ij}}\right)^{6}\right] + \frac{q_i q_j}{R_{ij}}\right\} \quad (1)$$

where r, θ, and φ are bond length, angle, and dihedral/improper angle, respectively, r_0 and θ_0 stand for the balance value; K is constant parameter, R_{ij} is the distance between the atoms i and j, and q is the charge. Lennard-Jones (LJ) parameters, σ and ε, between different atom types were obtained by using the Lorentz-Berthelot mixing rule:[20]

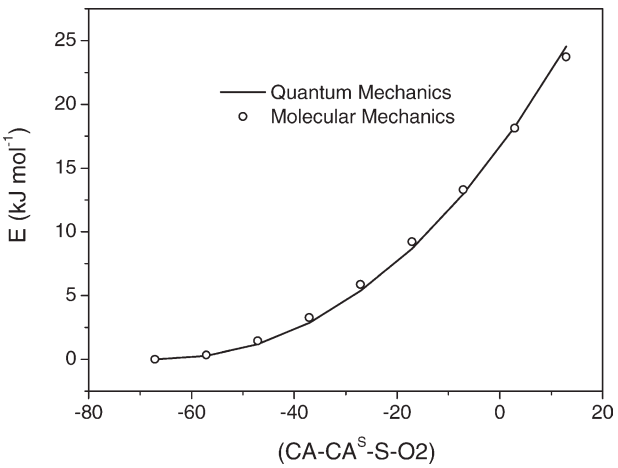

Figure 2. Torsion profile of CA-CA^S-S-O2 in $DBTO_2$.

Table 2. The Information of Simulated Systems

No.	Temperature	IL	Count	Water	Count	Model Compound	Count	Sulfur Content (ppm)	Simulation Box
1	300 K	$[C_{10}mim][PF_6]$	256	H_2O	–	DBT	9	3008	51.54
2	300/343 K	$[C_4mim][PF_6]$	256	H_2O	–	$DBTO_2$	7	3022	45.30/45.66
3	300 K	$[C_6mim][PF_6]$	256	H_2O	–	$DBTO_2$	8	3141	47.64
4	300 K	$[C_8mim][PF_6]$	256	H_2O	–	$DBTO_2$	9	3240	49.67
5	300 K	$[C_{10}mim][PF_6]$	256	H_2O	–	$DBTO_2$	9	2999	51.58
7	300 K	$[C_{10}mim][PF_6]$	256	H_2O	–	$DBTO_2$	2	667	51.35
8	300 K	$[C_{10}mim][PF_6]$	256	H_2O	–	$DBTO_2$	20	6503	51.96
9	343 K	$[C_{10}mim][PF_6]$	256	H_2O	–	$DBTO_2$	9	2999	50.24
10	300/343 K	$[C_{10}mim][BF_4]$	256	H_2O	–	$DBTO_2$	8	3162	50.38/50.85
11	343 K	$[C_{10}mim][PF_6]$	256	H_2O	90	$DBTO_2$	9	2994	52.38
12	343 K	$[C_{10}mim][BF_4]$	256	H_2O	80	$DBTO_2$	8	3156	51.09
13	343 K	$[C_4mim][PF_6]$	256	H_2O	70	$DBTO_2$	7	3017	45.99

$$\varepsilon_{ij} = \sqrt{\varepsilon_{ii}\varepsilon_{jj}} \qquad \sigma_{ij} = (\sigma_{ii} + \sigma_{jj})/2 \tag{2}$$

Force field parameters for ILs, composed by BF_4^-, PF_6^-, and $[C_nmim]^+$ (n = 4, 6, 8, 10) were obtained from Liu et al.[14]

The structures of DBT and $DBTO_2$ were optimized with the B3LYP[21,22]/6-31+G*[23] level using the Gaussian 03[24] program. Experimental bond and angle parameters for DBT have been added in Table 1. When compared with experimental data, it is found that most of the errors are less than 1.0%. The atom charges were fitted to reproduce the molecular electrostatic potentials, which were calculated at B3LYP[21,22]/6-311+G**[26] level. The fitting was carried out using restrained electrostatic potential (RESP) method.[27] Atomic partial charges, the equilibrium bonds, and angles obtained from the optimized structures are listed in Table 1. Atom types were assigned according to the AMBER force field, and all the atom types used in this work are shown in Figure 1.

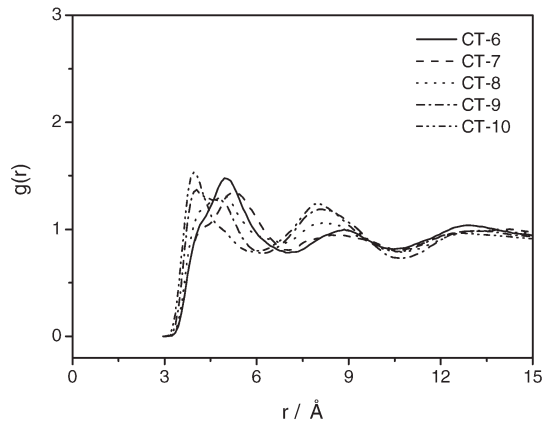

a) S atom in DBT and C atoms of side-chain in cation

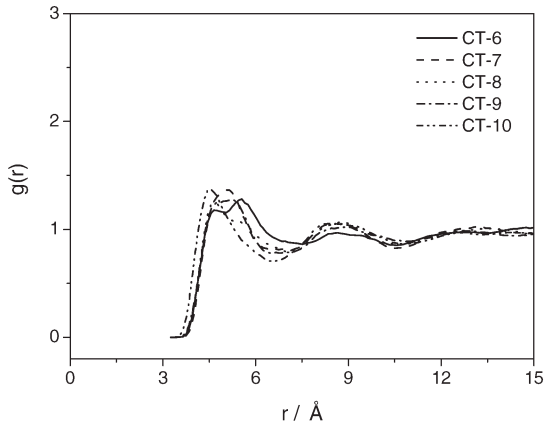

b) S atom in $DBTO_2$ and C atoms of side-chain in cation

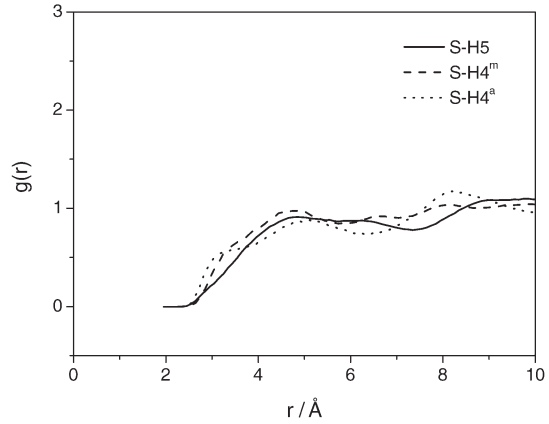

c) S atom in DBT and H atoms of imidazolium ring

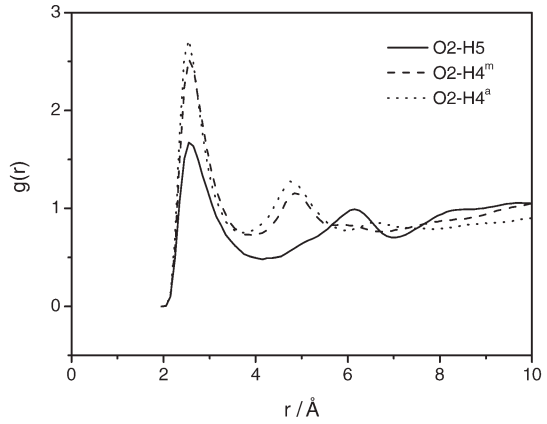

d) O atom in $DBTO_2$ and H atoms of imidazolium ring

Figure 3. RDFs between DBT/$DBTO_2$ and $[C_{10}mim][PF_6]$.

Table 3. Height and Location of First Peak for the RDFs Between DBT/$DBTO_2$ and $[C_{10}mim][PF_6]$

No.	Name 1	Name 2	RDF	H_{fp}	r_{fp} (Å)
1	$[C_{10}mim]^+$	DBT	CT6-S	1.48	4.95
2	$[C_{10}mim]^+$	DBT	CT7-S	1.34	5.35
3	$[C_{10}mim]^+$	DBT	CT8-S	1.31	4.95
4	$[C_{10}mim]^+$	DBT	CT9-S	1.37	4.05
5	$[C_{10}mim]^+$	DBT	CT10-S	1.53	3.95
6	$[C_{10}mim]^+$	$DBTO_2$	CT6-S	1.25	5.35
7	$[C_{10}mim]^+$	$DBTO_2$	CT7-S	1.37	5.05
8	$[C_{10}mim]^+$	$DBTO_2$	CT8-S	1.26	4.65
9	$[C_{10}mim]^+$	$DBTO_2$	CT9-S	1.28	5.25
10	$[C_{10}mim]^+$	$DBTO_2$	CT10-S	1.37	4.55
11	$[C_{10}mim]^+$	DBT	S-H5	0.91	4.85
12	$[C_{10}mim]^+$	DBT	S-$H4^m$	0.98	4.75
13	$[C_{10}mim]^+$	DBT	S-$H4^a$	0.87	4.85
14	$[C_{10}mim]^+$	$DBTO_2$	O2-H5	1.67	2.55
15	$[C_{10}mim]^+$	$DBTO_2$	O2-$H4^m$	2.52	2.55
16	$[C_{10}mim]^+$	$DBTO_2$	O2-$H4^a$	2.71	2.55

The bonding and bending parameters for the two model compounds were determined by fitting vibrational frequencies calculated by molecular mechanics (MM) to the experimental IR vibrational frequencies or the quantum mechanics (QM) frequencies calculated from the Gaussian 03 program. MM calculations were performed utilizing the TINKER package.[28] The B3LYP[21,22]/6-311+G**[26] method overestimates the frequencies by ~4%.[29] Therefore, a scaling factor of 0.96 is suitable for B3LYP[21,22]/6-311+G**[26] calculations.

We proposed and optimized the CA-CA-S-O2 dihedral parameter K_φ which is not included in AMBER.[19] γ parameter of the dihedral is derived from AMBER.[19] The ab initio torsion energy profiles were obtained using Gaussian 03 at the MP2[30]/6-311G**[26]//HF[31]/6-31+G*[26] level. The optimized conformers obtained from QM at various dihedral angles were used directly in MM energy calculations. Finally, the coefficients of the dihedrals were optimized by fitting the MM energy profiles to QM ones, and fitting for CA-CA-S-O2 is shown in Figure 2.

Simulation Details

Molecular dynamics (MD) simulations were performed with the standard periodical boundary conditions using the M.DynaMix program version 5.0.[32] Each system contained 256 $[C_n mim]^+$ cations, 256 anions, and different contents of model compounds. Table 2 shows the number of molecules in each system. Simulation started from an FCC lattice at a low density of 0.15 g/cm^3. When we simulated the mixture of ILs and sulfur compounds (or the mixture of IL, sulfur compound, and water), the two or three types of the molecules were put into the simulation box together. The initial positions of the molecules were generated randomly and the center of mass for each molecule was put on the FCC lattice point. After the system was relaxed in the NVE ensemble for a few MD steps (3000 steps) to remove possible overlap between molecules in the initial configuration, the Nose-Hoover[33] NpT ensemble was adopted with coupling constants of 100 fs for temperature and 700 fs for pressure, respectively. Then the system density was gradually increased to a reasonable value. The Tuckerman-Berne double time-step algorithm[34] was used with long- and short-time steps of 2 and 0.5 fs, respectively. The intramolecular forces were cut off at 15 Å, whereas the long range forces including LJ and Coulombic interactions were cut off at 20 Å, and Ewald[35] summation was implemented for the latter. The equilibration of the simulations was extended to 1.5 ns, and each production phase lasted for another 5.0 ns at 300 K or 343 K under 1.0 atm.

Results and Discussion

Liquid density

The density of DBT was used to validate the force field. The melting points of DBT and $DBTO_2$ are 370–373 K and 504–506 K, respectively, and the boiling point of DBT is 605–606 K.[36] Simulations were performed at 473 and 573 K for DBT and $DBTO_2$, respectively. The experimental and the calculated densities of DBT are 1.03 g/cm^3 and 1.01 g/cm^3, respectively, and the error is 1.9%. Molecular simulations for $DBTO_2$ were also performed, and the experimental and the calculated densities are 1.13 g/cm^3 and 1.10 g/cm^3, respectively, and the error is about 2.7%. The predicted density based on our proposed force field is in good agreement with the experimental data.

The above differences between experimental and computed results may be caused by several reasons. First, we noticed that trace amounts of impurities may change the value of the density dramatically.[16] Second, calculated atom charges may not be sufficient to accurately represent the distribution of charges in the real systems. Another possibility is that the LJ potential may not be realistic enough to describe interactions within these systems accurately.

Micro structure

First, interactions between $[C_{10}mim][PF_6]$ and the two model compounds at 300 K were studied by analyzing the radial distribution functions (RDFs), which are shown in Figure 3. Figures 3a, b present the RDFs between S atom in DBT/$DBTO_2$ and C atoms of the side chain in $[C_{10}mim]^+$. C10 is the end carbon, and in the order of gradually close to the imidazolium ring, C atoms are defined as C9, C8, C7, and C6. Table 3 shows the first peak height (H_{fp}) and location (r_{fp}) of the above RDFs for clarity. The heights of C-S RDFs for DBT are a bit higher than that for $DBTO_2$. From Figure 3c, it is obvious that the interaction between S in DBT and H in imidazolium ring is very weak. As is listed in Table 3, the H_{fp} decreases in the order of $H4^m > H5 > H4^a$, and that may be influenced by the alkyl chain. When comparing Figure 3a with Figure 3c, we can see that S atom in DBT prefer to surround the tail carbon atoms in $[C_{10}mim][PF_6]$, rather than H atoms in imidazolium ring. As is shown in Figure 3d, the strong interaction between O2 in $DBTO_2$ and H4*($H4^m$ or $H4^a$) in imidazolium ring may imply a hydrogen bond. When compared with $H4^m$, we found that the interaction strength between S and $H4^a$ is a little stronger, and that may be also influenced by the alkyl chain. When comparing Figure 3c with Figure 3d, it is obvious that $DBTO_2$ more easily to be extracted by ILs than DBT.

We analyzed several factors, which may influence the interaction between O2 in $DBTO_2$ and H in ILs, including side chain length, anion types, sulfur content, temperature,

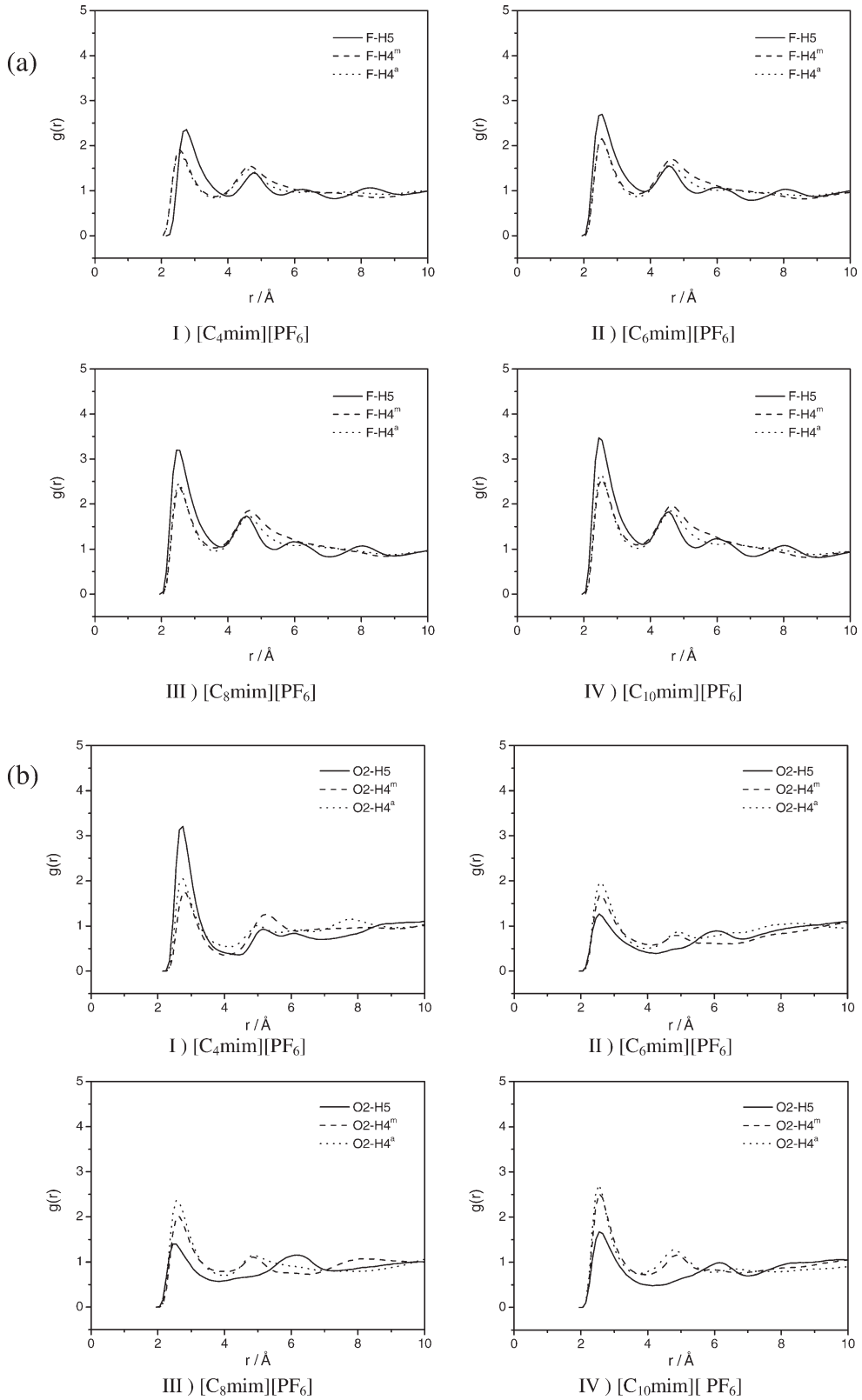

Figure 4. (a) RDFs between F atom in anion and H atoms in cation for [$C_n$mim][PF_6] (n = 4, 6, 8, 10). (b) RDFs between O in $DBTO_2$ and H in cation for [$C_n$mim][PF_6] (n = 4, 6, 8, 10).

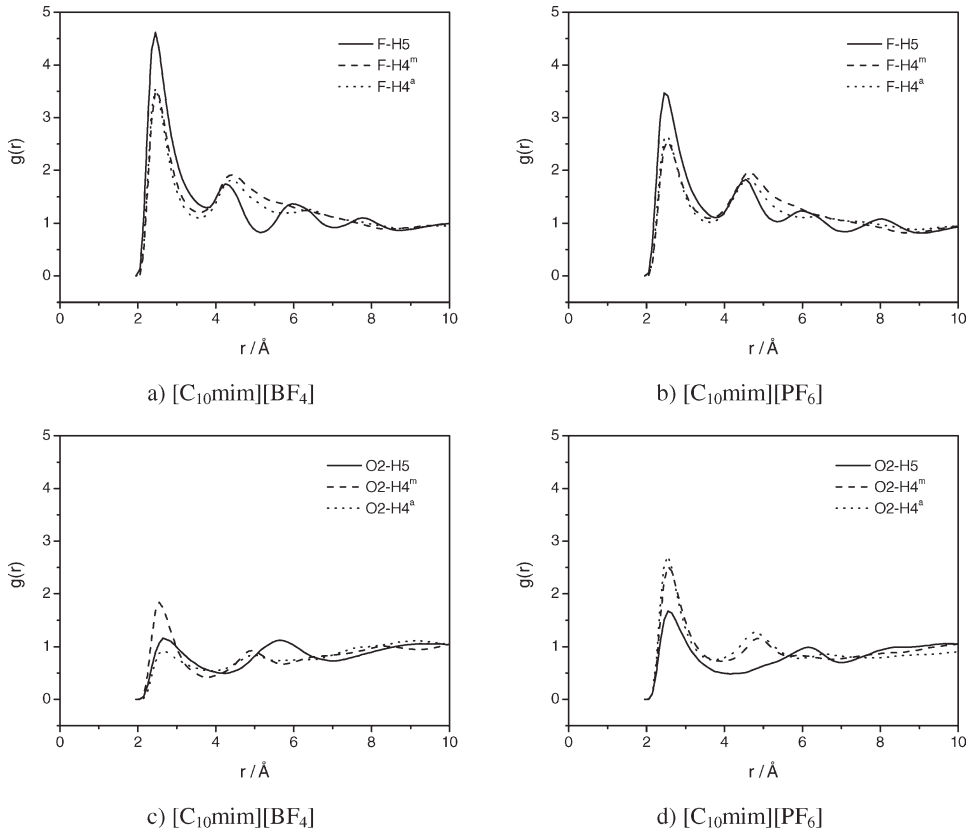

Figure 5. RDFs of F atom in anion and H atoms in cation, [C_{10}mim][BF_4] (a) and [C_{10}mim][PF_6] (b). RDFs of O atom in $DBTO_2$ and H atoms in cation, [C_{10}mim][BF_4] (c) and [C_{10}mim][PF_6] (d).

Table 4. Height and Location of First Peak for the RDFs of F-HX and O2-HX for [$C_n$mim][PF_6] (n = 4, 6, 8, 10)

F-HX						
	F-H5		F-H4^m		F-H4^a	
RDFs	H_{fp}	r_{fp} (Å)	H_{fp}	r_{fp} (Å)	H_{fp}	r_{fp} (Å)
[C_4mim][PF_6]	2.36	2.75	1.92	2.55	1.85	2.55
[C_6mim][PF_6]	2.69	2.55	2.15	2.55	2.16	2.55
[C_8mim][PF_6]	3.19	2.45	2.38	2.55	2.47	2.55
[C_{10}mim][PF_6]	3.47	2.45	2.56	2.55	2.66	2.55

O2-HX						
	O2-H5		O2-H4^m		O2-H4^a	
RDFs	H_{fp}	r_{fp} (Å)	H_{fp}	r_{fp} (Å)	H_{fp}	r_{fp} (Å)
[C_4mim][PF_6]	3.21	2.75	1.74	2.75	2.05	2.75
[C_6mim][PF_6]	1.27	2.55	1.67	2.55	1.95	2.55
[C_8mim][PF_6]	1.40	2.45	2.01	2.65	2.36	2.55
[C_{10}mim][PF_6]	1.67	2.55	2.52	2.55	2.71	2.55

Table 5. First Peak Height and Location of F-HX and O2-HX RDFs for [C_{10}mim][BF_4] and [C_{10}mim][PF_6]

	F-H5		F-H4^m		F-H4^a	
RDFs	H_{fp}	r_{fp} (Å)	H_{fp}	r_{fp} (Å)	H_{fp}	r_{fp} (Å)
[C_{10}mim][BF_4]	4.62	2.45	3.51	2.45	3.55	2.45
[C_{10}mim][PF_6]	3.47	2.45	2.56	2.55	2.66	2.55

	O2-H5		O2-H4^m		O2-H4^a	
RDFs	H_{fp}	r_{fp} (Å)	H_{fp}	r_{fp} (Å)	H_{fp}	r_{fp} (Å)
[C_{10}mim][BF_4]	1.16	2.65	1.84	2.55	0.92	2.65
[C_{10}mim][PF_6]	1.67	2.55	2.52	2.55	2.71	2.55

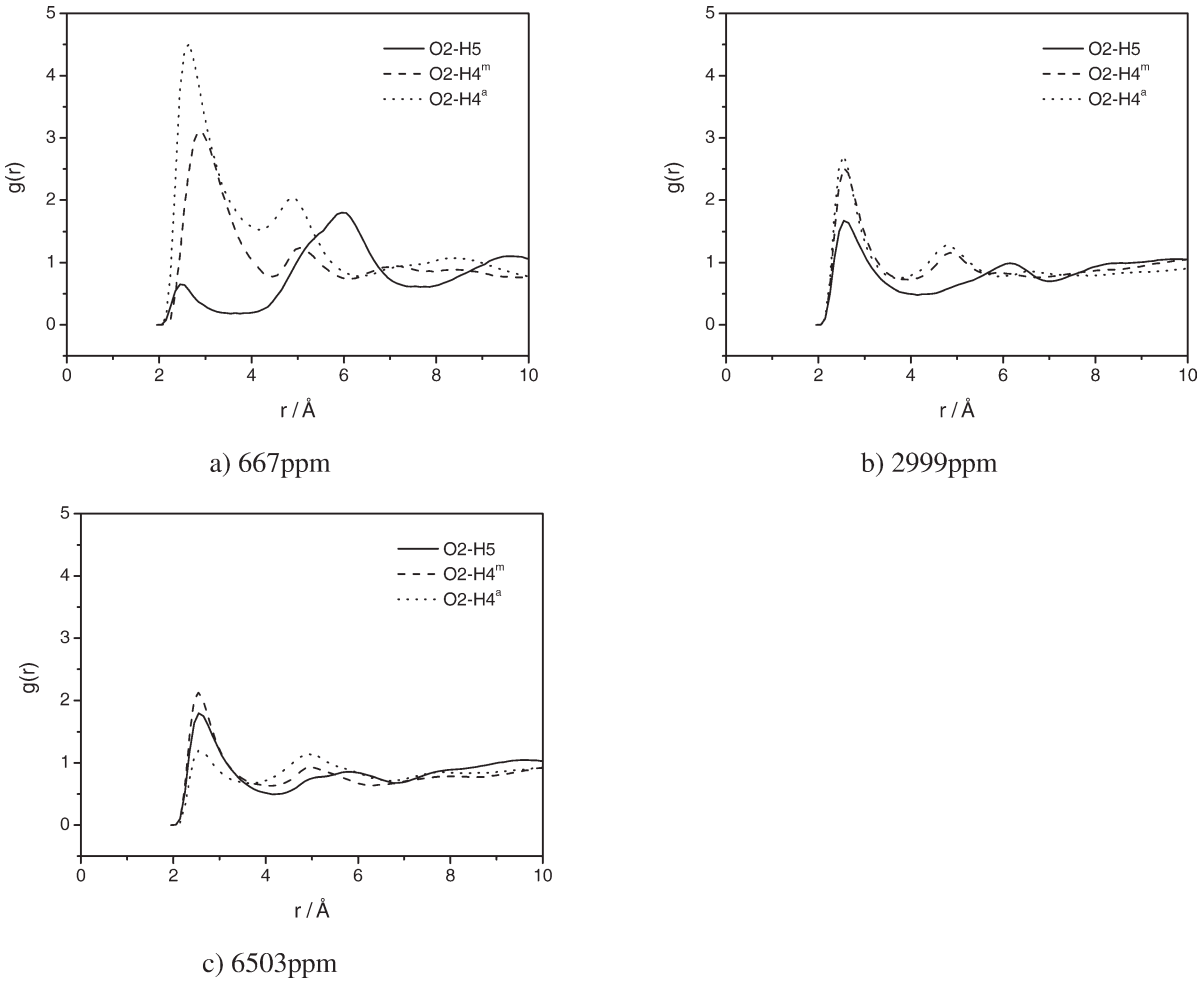

Figure 6. RDFs of O atom in $DBTO_2$ and H atoms in cation for $[C_{10}mim][PF_6]$ with different sulfur contents.

and water. All the results are provided in detail in the following sections.

Cation. Bösmann et al.[1] experimentally studied the cation and anion effects on desulfurization by ILs. They concluded that the size of the ions greatly affects extraction, and cations are proved to be more important.[1] In this work, a series of 1-alkyl-3-methylimidazolium ILs, $[C_n mim][PF_6]$ (n = 4–10) were used as extractants to study the influence of side chain length at 300 K. RDFs between the F atom in the anion and HX (H5, $H4^a$, or $H4^m$) in the cation with different side chain length are shown in Figure 4a. We can see that the interactions between the F atom in $[PF_6]^-$ and the H atoms in imidazolium ring become stronger with increasing side chain length, ($n >$ 4). It is the same with the other researchers' results.[12] Molecular volume of $DBTO_2$ is much bigger than that of $[PF_6]^-$, so the steric hindrance effect becomes more obvious for $DBTO_2$. As a result, the interaction between $DBTO_2$ and $[C_4mim][PF_6]$ is larger than that of $[C_6mim][PF_6]$.

As is shown in Figure 4 and Table 4, the interaction between F and H5 is stronger than that between F and H4* ($H4^a$ or $H4^m$). It is difficult for O2 atoms in $DBTO_2$ to replace the F atom in $[PF_6]^-$ which could form a hydrogen bond with H5. From Figure 4b, we can see that the height of RDFs between O2 and H4 ($H4^a$ or $H4^m$) is higher than that between O2 and H5 in $[C_n mim][PF_6]$ (n = 6–10). As the interaction between F and H5 is weaker for $[C_4mim][PF_6]$, the H_{fp} of O2-H5 RDF is still higher than the other two RDFs.

Anion. We investigated the effect of anions by performing simulations at 300 K for $DBTO_2$ with two kinds of ILs, $[C_{10}mim][PF_6]$ and $[C_{10}mim][BF_4]$, respectively. As is seen in Figures 5a, b, the interaction between F and HX in $[C_{10}mim][PF_6]$ is weaker than that in $[C_{10}mim][BF_4]$. When comparing the F atom charges in the two anions ($[PF_6]^-$: -0.2927; $[BF_4]^-$: -0.5376),[14] it is obvious that the HX could form hydrogen bonds easily for $[C_{10}mim][BF_4]$. After careful examination of Figure 5 and Table 5, we found a mutual yin and yang behavior. That is when F-HX

Table 6. First Peak Height and Location of O2-HX RDFs for Different Sulfur Content

	O2-H5		O2-$H4^m$		O2-$H4^a$	
RDFs	H_{fp}	r_{fp} (Å)	H_{fp}	r_{fp} (Å)	H_{fp}	r_{fp} (Å)
667 ppm	0.65	2.45	3.12	2.85	4.51	2.65
2999 ppm	1.67	2.55	2.52	2.55	2.71	2.55
6503 ppm	1.80	2.55	2.13	2.55	1.20	2.55

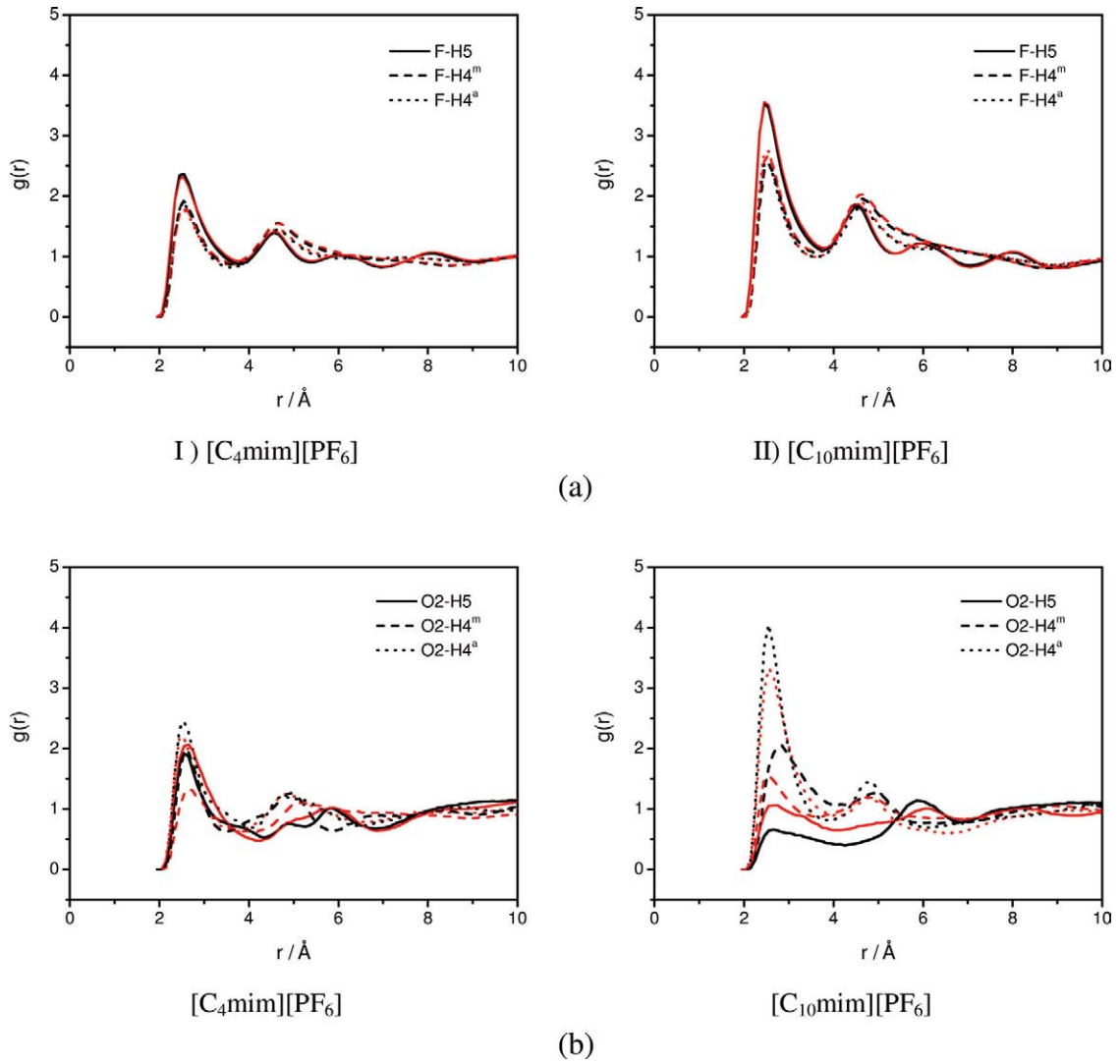

Figure 7. (a) RDFs between F atom in anion and H atoms in cation for IL and $DBTO_2$ system at 343 K (black) and 300 K (red). (b) RDFs between O atom in $DBTO_2$ and H atoms in cation for IL and $DBTO_2$ system at 343 K (black) and 300 K (red).

[Color figure can be viewed in the online issue, which is available at wileyonlinelibrary.com.]

interaction is weaker, the O2-HX interaction is stronger and vice versa. When comparing Figure 5c with Figure 5d, we found it is easy for O2 in $DBTO_2$ to form a hydrogen bond with the HX in imidazolium ring of $[C_{10}mim][PF_6]$. Therefore, when compared with $[C_{10}mim][BF_4]$, $[C_{10}mim][PF_6]$ is a better solvent for extracting $DBTO_2$ from fuel oil. The conclusion was also proved experimentally by Zhu et al.[8]

Table 7. First Peak Height and Location of F-HX and O2-HX RDFs at 343 K

	F-H5		F-H4^m		F-H4^a	
RDFs	H_{fp}	r_{fp} (Å)	H_{fp}	r_{fp} (Å)	H_{fp}	r_{fp} (Å)
$[C_4mim][PF_6]$	2.30	2.55	1.83	2.55	1.77	2.55
$[C_{10}mim][PF_6]$	3.36	2.45	2.42	2.55	2.58	2.55
$[C_{10}mim][BF_4]$	4.47	2.45	3.30	2.45	3.47	2.45
	O2-H5		O2-H4^m		O2-H4^a	
RDFs	H_{fp}	r_{fp} (Å)	H_{fp}	r_{fp} (Å)	H_{fp}	r_{fp} (Å)
$[C_4mim][PF_6]$	1.86	2.65	1.85	2.65	1.79	2.55
$[C_{10}mim][PF_6]$	1.55	2.55	1.88	2.65	2.05	2.55
$[C_{10}mim][BF_4]$	1.18	2.55	2.01	2.55	1.19	2.55

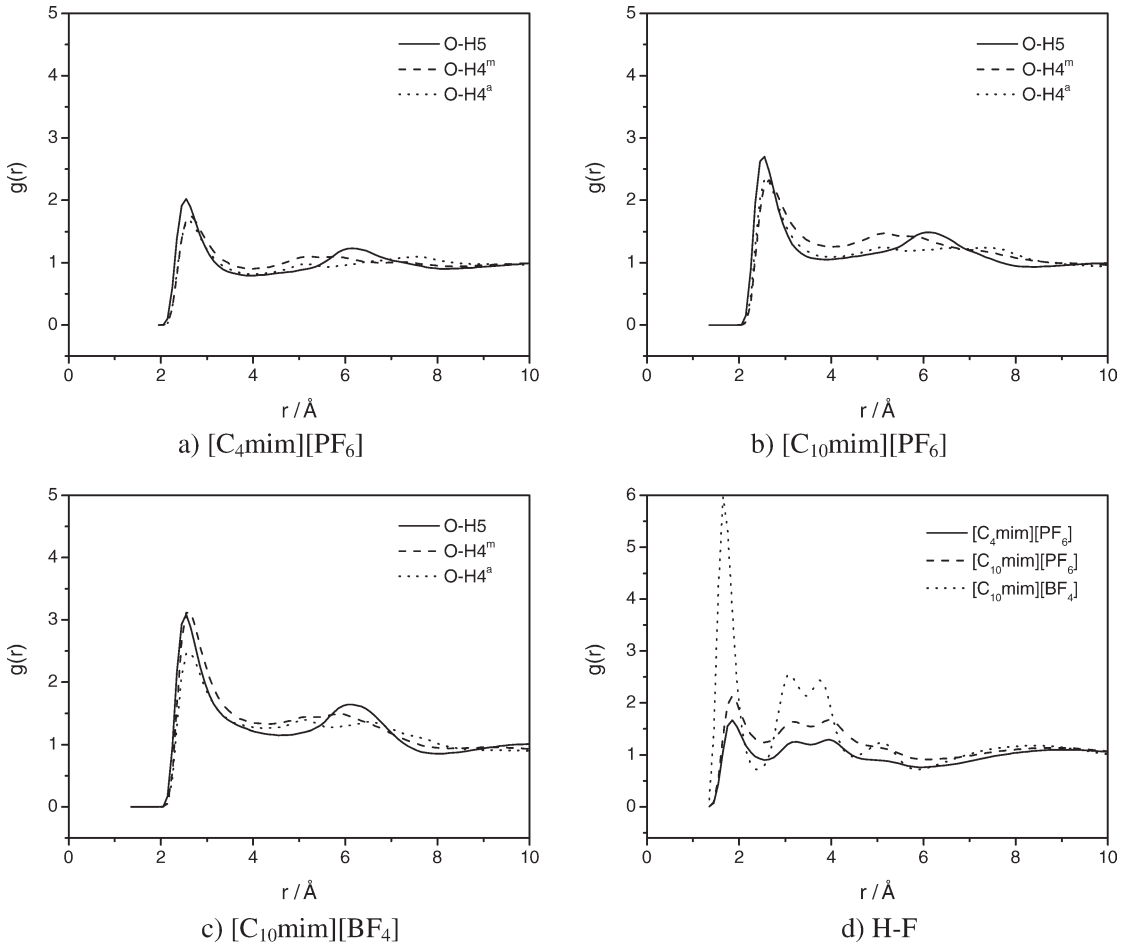

Figure 8. RDFs between O atom in H_2O and H atoms in cation for different ILs. [C_4mim][PF_6] (a), [C_{10}mim][PF_6] (b), and [C_{10}mim][BF_4] (c). RDFs between H atom in H_2O and F atom in anion for different ILs (d).

Sulfur Content. Simulations were performed at 300 K for [C_{10}mim][PF_6] under three kinds of sulfur contents, and the RDFs for O atom in $DBTO_2$ and HX in $[C_{10}mim]^+$ are shown in Figure 6. For clarity, the H_{fp} and r_{fp} are listed in Table 6. We found that the interaction strength for O2-H4^a and O2-H4^m decrease with increasing the sulfur content, and the decrease is more obvious for O2-H4^a. However, the H_{fp} for O2-H5 becomes higher with increasing the sulfur content. The above results may imply that the $DBTO_2$ molecules are too far away to interact with each other when the $DBTO_2$ content is low enough. However, the interactions for O2-H4^a, O2-H4^m, and O2-H5 become average with higher $DBTO_2$ contents.

Temperature. Simulations were carried out at 343 K for [C_4mim][PF_6] and [C_{10}mim][PF_6] mixed with $DBTO_2$, respectively. When compared with the results under 300 K (Figures 4 and 5), it can be seen that the interaction strength between H and F decreases very little with the temperature increasing (Figure 7a and Table 7). In contrast, the interaction between H and O2 becomes weaker obviously especially for [C_4mim][PF_6]. On the other hand, temperature also has some effects on the mass transfer. For example, based on our previous work on phosphonium-based ILs,[37] we found that ILs move very slowly at low temperatures, and the transfer will be faster at the higher temperatures. Zhu et al.[8] experimentally found that higher temperature is better

Table 8. First Peak Height and Location of O-HX and H-F RDFs in Aqueous System

	O-H5		O-H4^m		O-H4^a		H-F	
RDFs	H_{fp}	r_{fp} (Å)	H_{fp}	r_{fp} (Å)	H_{fp}	r_{fp} (Å)	H_{fp}	r_{fp} (Å)
[C_4mim][PF_6]	2.02	2.55	1.75	2.65	1.66	2.65	1.67	1.85
[C_{10}mim][PF_6]	2.70	2.55	2.25	2.55	2.34	2.55	2.14	1.85
[C_{10}mim][BF_4]	3.09	2.55	3.12	2.55	2.48	2.65	5.97	1.65

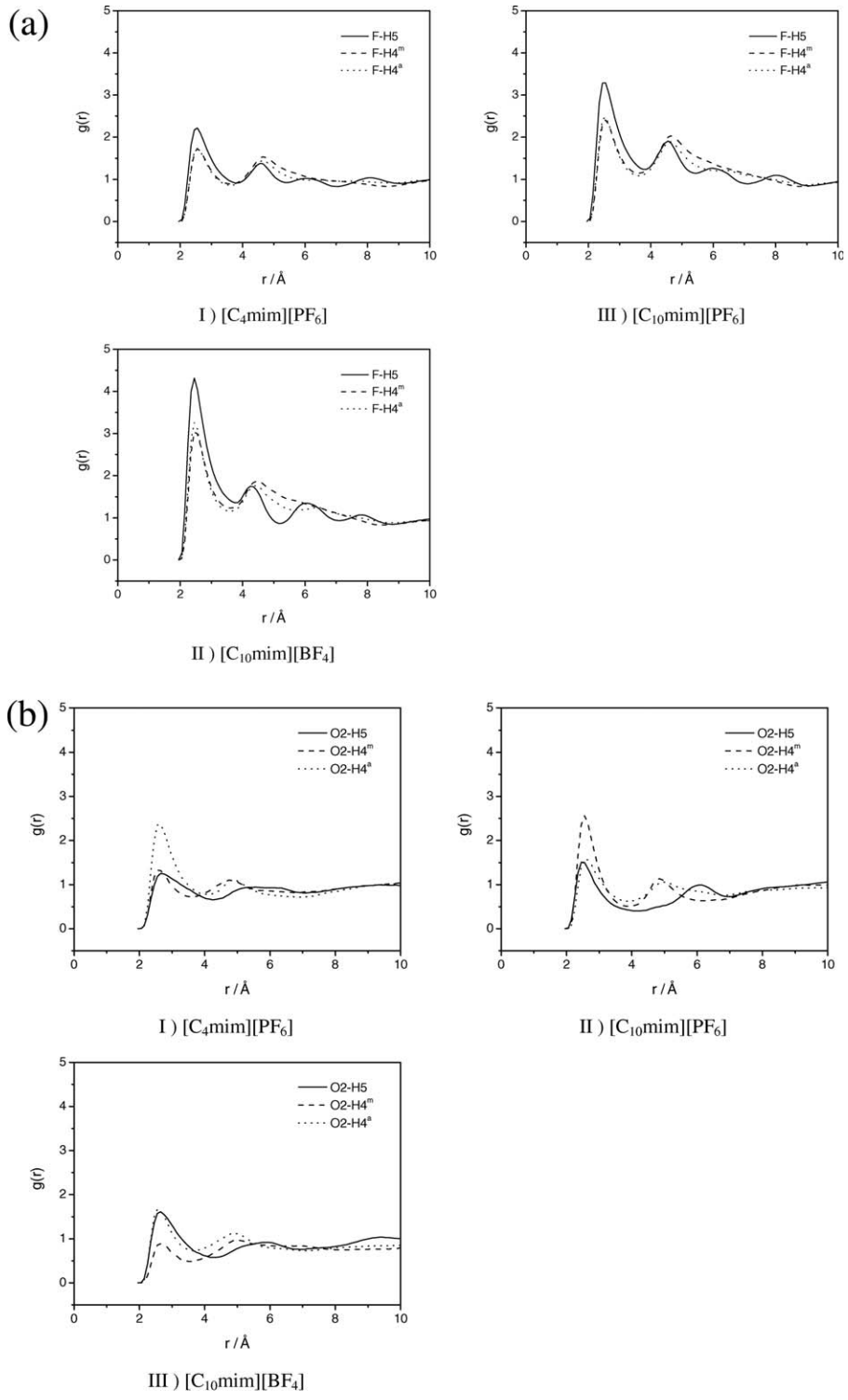

Figure 9. (a) RDFs between F atom in anion and H atoms in cation in aqueous system. (b) RDFs between O atom in $DBTO_2$ and H atoms in cation in aqueous system.

for desulfurization. That may be caused by the lower viscosities for the ILs at higher temperatures.

Water Content. The IL and $DBTO_2$ aqueous system was simulated at 343 K. The mole ratio of $DBTO_2$:H_2O was 1:10. First, the interaction between IL and H_2O was analyzed, as shown in Figure 8. The peak heights of RDFs between O in H_2O and HX in imidazolium ring of $[C_{10}mim]^+$ is higher than that of $[C_4mim]^+$, as shown in

Table 9. First Peak Height and Location of F-HX and O2-HX RDFs in Aqueous System

	F-H5		F-H4^m		F-H4^a	
RDFs	H_{fp}	r_{fp} (Å)	H_{fp}	r_{fp}(Å)	H_{fp}	r_{fp} (Å)
$[C_4mim][PF_6]$	2.22	2.55	1.73	2.55	1.74	2.55
$[C_{10}mim][BF_4]$	4.31	2.45	3.04	2.45	3.26	2.45
$[C_{10}mim][PF_6]$	3.29	2.55	2.42	2.55	2.48	2.55
	O2-H5		O2-H4^m		O2-H4^a	
RDFs	H_{fp}	r_{fp} (Å)	H_{fp}	r_{fp} (Å)	H_{fp}	r_{fp} (Å)
$[C_4mim][PF_6]$	1.25	2.65	1.32	2.55	2.36	2.65
$[C_{10}mim][BF_4]$	1.61	2.65	0.89	2.65	1.67	2.55
$[C_{10}mim][PF_6]$	1.51	2.45	2.56	2.55	1.58	2.55

Figures 8a, b. When comparing the three kinds of ILs, we found that the interaction strength increases in the order of $[C_4mim][PF_6] < [C_{10}mim][PF_6] < [C_{10}mim][BF_4]$, and that can be also concluded from Table 8. Besides, the interaction between H in H_2O and F in $[BF_4]^-$ is much stronger than that of $[PF_6]^-$, as shown in Figure 8d.

Figure 9 is the plot of RDFs for HX-F and HX-O2. When compared with the pure IL (Figure 7), it can be seen that the H_{fp} for HX-F decreases a little in the aqueous system. It may be an implication that the interaction strength between cation and anion becomes weaker induced by water. However, no obvious change has been found for HX-O2 RDFs, and it may be caused by water forms hydrogen bonds with HX in the imidazolium ring, which also interacts with the O2 in $DBTO_2$.

To determine more information about the interaction between IL and $DBTO_2$ in aqueous system, the hydrogen bond angle distribution was also studied. Generally, if the distance between the H atom in cation and the O2 atom in DBTO2 (C—H···O2) is less than the sum of H and O2 van

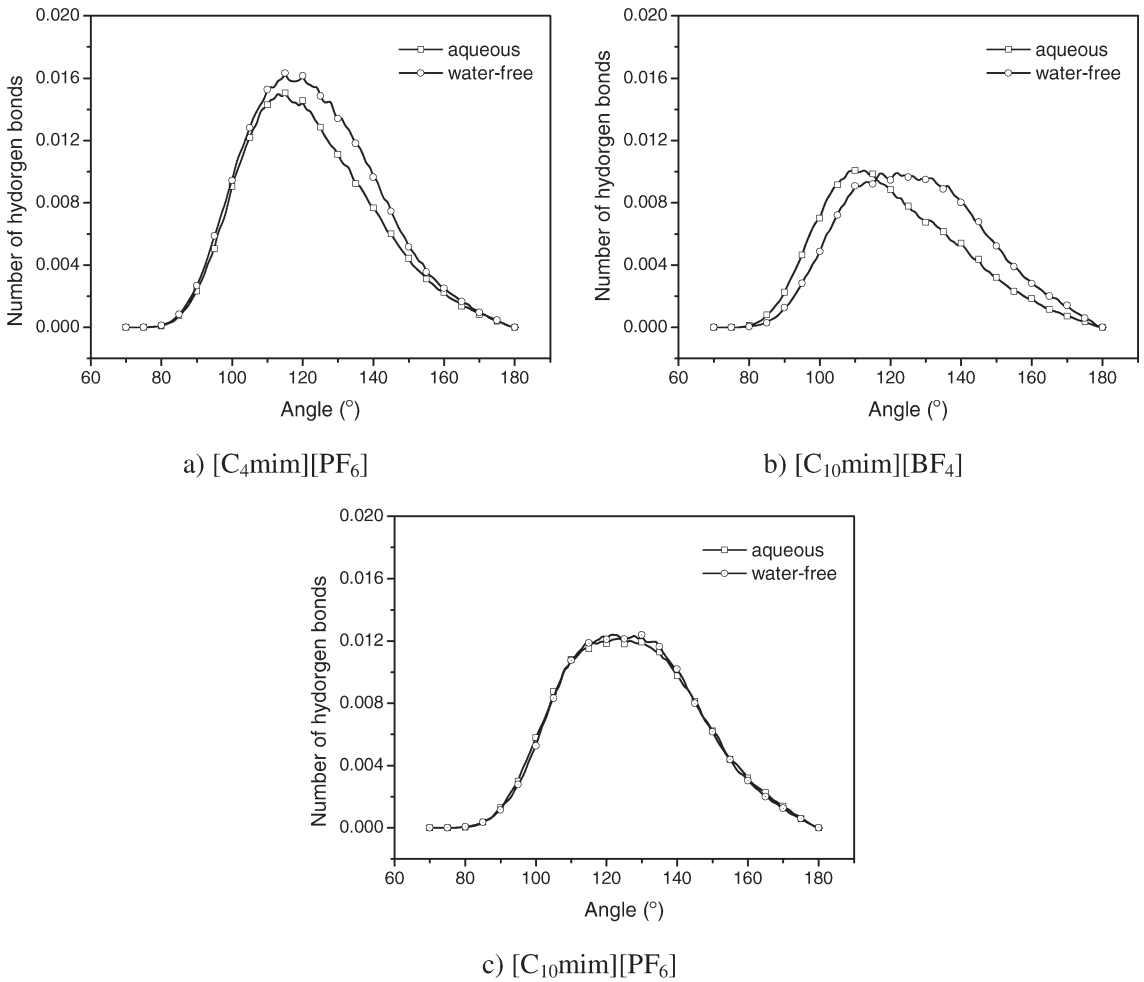

a) $[C_4mim][PF_6]$

b) $[C_{10}mim][BF_4]$

c) $[C_{10}mim][PF_6]$

Figure 10. The C—H···O2 hydrogen bond angle distribution of IL and $DBTO_2$ in aqueous system.

der Waals radii, and the C—H···O2 angle is greater than 90°, it indicates H···O2 hydrogen bonding.[38,39] Thus the C—H···O2 hydrogen bond distances should be less than 2.70 Å. According to this principle, we calculated the hydrogen bond angle distribution for different systems and showed the results in Figure 10. When compared with the water-free systems, the hydrogen bond angle distributions change differently for the three kinds of ILs in aqueous system. For $[C_{10}mim][PF_6]$, the peak of hydrogen bond angle move toward the larger angle. However, nearly no change is obvious for $[C_{10}mim][BF_4]$. In case of $[C_4mim][PF_6]$, the location of peak changes very little. In a word, addition of little water may have some positive effects on the extractive desulfurization by hydrophilic ILs, just like $[C_{10}mim][BF_4]$.

Conclusions

A force field was set up and validate for dibenzothiophene (DBT) and dibenzothiophene 5,5-dioxide ($DBTO_2$). The mechanism of desulphurization was studied by MD simulation using DBT and $DBTO_2$ as the model compounds. We depicted the interaction between the model compounds and a series of 1-alkyl-3-methylimidazolium ILs ($[C_nmim]^+$, n = 4–10). We found that the O2 in $DBTO_2$ will form a strong hydrogen bond with the H in the imidazolium ring. As NMR would be a powerful tool to check the hydrogen bond, we will consider it for future research. Thus, $DBTO_2$ is extracted by ILs more easily than DBT. The H4*($H4^m$ or $H4^a$)-O2 hydrogen bond strength order for different alkyl side chains of the cations is $[C_{10}mim]^+ > [C_8mim]^+ > [C_4mim]^+ > [C_6mim]^+$. When comparing ILs with different anions, $[C_{10}mim][PF_6]$ and $[C_{10}mim][BF_4]$, the hydrogen bond strength between O2 and H4* of the former IL is stronger than that of the latter one. The above conclusions may be helpful to guiding the selection of extractant, and the result of sulfur content, water and temperature effects on desulphurization will help us to chose the operating conditions. In the future, the interaction between other model sulfur components and ILs will be studied and more operating conditions will be also considered.

Acknowledgments

This work was supported by the National Science Fund of China for Distinguished Young Scholar (20625618), National Basic Research Program of China (2009CB219902), and National Natural Scientific Fund of China (20903098).

Literature Cited

1. Bösmann A, Datsevich L, Jess A, Lauter A, Schmitz C, Wasserscheid P. Deep desulfurization of diesel fuel by extraction with ionic liquids. *Chem Commun*. 2001;1:2494–2495.
2. Zhang S, Zhang Z. Novel properties of ionic liquids in selective sulfur removal from fuels at room temperature. *Green Chem*. 2002;4: 376–379.
3. Su B, Zhang S, Zhang C. Structural elucidation of thiophene interaction with ionic liquids by multinuclear NMR spectroscopy. *J Phys Chem B*. 2004;108:19510–19517.
4. Zhang S, Zhang Q, Zhang Z. Extractive desulfurization and denitrogenation of fuels using ionic liquids. *Ind Eng Chem Res*. 2004;43: 614–622.
5. Carrado KA, Kim JH, Song CS, Castagnola N, Marshall CL, Schwartz MM. HDS and deep HDS activity of CoMoS-mesostructured clay catalysts. *Catal Today*. 2006;116:478–484.
6. Nie Y, Li C, Sun A, Meng H, Wang Z. Extractive desulfurization of gasoline using imidazolum based phosphoric ionic liquids. *Energy Fuels*. 2006;20:2083–2087.
7. Ma X, Zhou A, Song C. A novel method for oxidative desulfurization of liquid hydrocarbon fuels based on catalytic oxidation using molecular oxygen coupled with selective adsorption. *Catal Today*. 2007;123:276–284.
8. Zhu W, Li H, Jiang X, Yan Y, Lu J, Xia J. Oxidative desulfurization of fuels catalyzed by peroxotungsten and peroxomolybdenum complexes in ionic liquids. *Energy Fuels*. 2007;21: 2514–2516.
9. Cassol C, Umpierre A, Ebeling G, Ferrera B, Chiaro S, Dupont J. On the extraction of aromatic compounds from hydrocarbons by imidazolium ionic liquids. *Int J Mol Sci*. 2007;8:593–605.
10. Morrow TI, Maginn EJ. Molecular dynamics study of the ionic liquid 1-*n*-butyl-3-methylimidazolium hexafluorophosphate. *J Phys Chem B*. 2002;106:12807–12813.
11. Lopes JNAC, Pádua AAH. Molecular force field for ionic liquids composed of the triflate or bistriflylimide anions. *J Phys Chem B*. 2004;108:16893–16898.
12. Lopes JNAC, Pádua AAH. Nanostructural organization in ionic liquids. *J Phys Chem B*. 2006;110:3330–3335.
13. Zhou G, Liu X, Zhang S, Yu G, He H. A force field for molecular simulation of tetrabutylphosphonium amino acid ionic liquids. *J Phys Chem B*. 2007;111:7078–7084.
14. Liu Z, Huang S, Wang W. A refined force field for molecular simulation of imidazolium-based ionic liquids. *J Phys Chem B*. 2004; 108:12978–12989.
15. Liu X, Zhou G, Zhang S, Wu G, Yu G. Molecular simulation of guanidinium-based ionic liquids. *J Phys Chem B*. 2007;111:5658–5668.
16. Liu X, Zhang S, Zhou G, Wu G, Yuan X, Yao X. New force field for molecular simulation of guanidinium-based ionic liquids. *J Phys Chem B*. 2006;110:12062–12071.
17. Cadena C, Zhao Q, Snurr RQ, Maginn EJ. Molecular modeling and experimental studies of the thermodynamic and transport properties of pyridinium-based ionic liquids. *J Phys Chem B*. 2006;110:2821–2832.
18. Yu G, Zhang S, Zhou G, Liu X, Chen X. Structure, interaction and property of amino-functionalized imidazolium ILs by molecular dynamics simulation and Ab initio calculation. *AIChE J*. 2007;53: 3210–3221.
19. Cornell WD, Cieplak P, Bayly CI, Gould IR, Merz KM Jr, Ferguson DM, Spellmeyer DC, Fox T, Caldwell JW, Kollman PA. A second generation force field for the simulation of proteins, nucleic acids, and organic molecules. *J Am Chem Soc*. 1995;117:5179–5197.
20. Allen MP, Tildesley DJ. *Computer Simulations of Liquids*. Oxford: Clarendon Press, 1987.
21. Becke AD. Density-functional thermochemistry. III. The role of exact exchange. *J Chem Phys*. 1993;98:5648–5652.
22. Stephens PJ, Devlin FJ, Chabalowski CF, Frisch MJ. Ab initio calculation of vibrational absorption and circular dichroism spectra using density functional force fields. *J Phys Chem*. 1994;98:11623–11627.
23. Hehre WJ, Ditchfield R, Pople JA. Self-consistent molecular orbital methods. xii. Further extensions of gaussian-type basis sets for use in molecular orbital studies of organic molecules. *J Chem Phys*. 1972;56:2257–2262.
24. Frisch MJ, Trucks GW, Schlegel HB, Scuseria GE, Robb MA, Cheeseman JR, Montgomery JA, Vreven T, Kudin KN, Burant JC, Millam JM, Iyengar SS, Tomasi J, Barone V, Mennucci B, Cossi M, Scalmani G, Rega N, Petersson GA, Nakatsuji H, Hada M, Ehara M, Toyota K, Fukuda R, Hasegawa J, Ishida M, Nakajima T, Honda Y, Kitao O, Nakai H, Klene M, Li X, Knox JE, Hratchian HP, Cross JB, Adamo C, Jaramillo J, Gomperts R, Stratmann RE, Yazyev O, Austin AJ, Cammi R, Pomelli C, Ochterski JW, Ayala PY, Morokuma K, Voth GA, Salvador P, Dannenberg JJ, Zakrzewski VG, Dapprich S, Daniels AD, Strain MC, Farkas O, Malick DK, Rabuck AD, Raghavachari K, Foresman JB, Ortiz JV, Cui Q, Baboul AG, Clifford S, Cioslowski J, Stefanov BB, Liu G, Liashenko A, Piskorz P, Komaromi I, Martin RL, Fox DJ, Keith T, Al-Laham MA, Peng CY, Nanayakkara A, Challacombe M, Gill PMW, Johnson B, Chen W, Wong MW, Gonzalez C, Pople JA. *Gaussian 03, Revision C. 02*. Wallingford, CT: Gaussian, Inc., 2004.

25. Schaffrin R, Trotter J. Structure of dibenzothiophen. *J Chem Soc A*. 1970;9:1561–1565.
26. Raghavachari K, Binkley JS, Seeger R, Pople JA. Self-consistent molecular orbital methods. 20. Basis set for correlated wave-functions. *J Chem Phys*. 1980;72:650–654.
27. Bayly CI, Cieplak P, Cornell WD, Kollman PA. A well-behaved electrostatic potential based method using charge restraints for deriving atomic charges: the RESP model. *J Phys Chem*. 1993;97:10269–10280.
28. Pappu R, Hart R, Ponder J. Analysis and application of potential energy smoothing for global optimization. *J Phys Chem B*. 1998; 102:9725–9742.
29. Lii J-H, Allinger NL. Molecular mechanics. The MM3 force field for hydrocarbons. 2. Vibrational frequencies and thermodynamics. *J Am Chem Soc*. 1989;111:8566–8575.
30. Frisch MJ, Head-Gordon M, Pople JA. Semi-direct algorithms for the MP2 energy and gradient. *Chem Phys Lett*. 1990;166:281–289.
31. Pople JA, Nesbet RK. Self-consistent orbitals for radicals. *J Chem Phys*. 1954;22:571–572.
32. Lyubartsev AP, Laaksonen A. M.DynaMix—a scalable portable parallel MD simulation package for arbitrary molecular mixtures. *Comput Phys Commun*. 2000;128:565–589.
33. Martyna GJ, Tuckerman M, Tobias DJ, Klein ML. Explicit reversible integrators for extended systems dynamics. *Mol Phys*. 1996;87: 1117–1157.
34. Tuckerman M, Berne BJ, Martyna GJ. Reversible multiple time scale molecular dynamics. *J Chem Phys*. 1992;97:1990–2001.
35. De Leeuw SW, Perram JW, Smith ER. Simulation of electrostatic systems in periodic boundary conditions. III. Further theory and applications. *Proc R Soc Lond A Math Phys Eng Sci*. 1983;388:177–193.
36. Available at: http://www.chemicalbook.com/ProductChemicalPropertiesCB7426957_EN.htm.
37. Liu X, Zhou G, Zhang S, Yu G. Molecular simulations of phosphonium-based ionic liquid. *Mol Simul*. 2010;36:79–86.
38. Taylor R, Kennard O. Crystallographic evidence for the existence of C—H···O, C—H···N, and C—H···Cl hydrogen bonds. *J Am Chem Soc*. 1982;104:5063–5070.
39. Fuller J, Carlin R, Long H, Hawotth D. Structure of 1-ethyl-3-methylimidazolium hexafluorophosphate: model for room temperature molten salts. *J Chem Soc Chem Commun*. 1994;3:299–300.

Manuscript received Feb. 18, 2009, and revision received Jan. 1, 2010.